Optimization of MEMS Vibration Energy Harvester With Perforated Electrode

Anxin Luo, Yulong Zhang, Xinge Guo, *Graduate Student Member, IEEE*, Yan Lu, *Senior Member, IEEE*, Chengkuo Lee, *Senior Member, IEEE*, and Fei Wang, *Senior Member, IEEE*

***Abstract*— In this paper, electret based vibration energy harvesters are designed and fabricated with perforated electrode based on MEMS technology. Through-holes are distributed on the fixed electrode in the device to optimize the energy harvesting process. The effect of the holes on the output power of the device are analyzed and discussed both in the finite element method (FEM) simulation and the experiments. It can be noticed that the through-holes can effectively lower the squeeze-film air damping force on the moveable proof mass at the atmosphere. Therefore, the energy loss due to the air damping could be reduced, and the output power of the device increases. The effects of the hole diameter and numbers on the output power of our device are also investigated in detail. By optimizing the configuration of the holes, the perforated device with the hole diameter of 400 μm and depth of 100 μm exhibits the highest power output at the low acceleration of 1.84 m/s^2, which proves promising application for self-powered electronics in the future. [2020-0380]**

Manuscript received December 9, 2020; revised January 18, 2021; accepted January 26, 2021. Date of publication February 22, 2021; date of current version March 16, 2021. This work was supported in part by the Shenzhen Science and Technology Innovation Committee under Grant JCYJ20200109105838951 and in part by the Guangdong Natural Science Funds under Grant 2016A030306042 and Grant 2018A050506001. Subject Editor A. Zhang. *(Anxin Luo and Yulong Zhang contributed equally to this work.) (Corresponding author: Fei Wang.)*

Anxin Luo is with the School of Microelectronics, Southern University of Science and Technology (SUSTech), Shenzhen 518055, China, also with the Research Center of Integrated Circuits for Next-Generation Communications, Ministry of Education, Southern University of Science and Technology (SUSTech), Shenzhen 518055, China, also with the Institute of Microelectronics, University of Macau (UM), Taipa, Macau, also with the State Key Laboratory of Analog and Mixed-Signal VLSI, University of Macau (UM), Taipa, Macau, and also with the Department of Electrical and Computer Engineering, Faculty of Science and Technology, University of Macau (UM), Taipa, Macau (e-mail: luoax@mail.sustech.edu.cn).

Yulong Zhang is with the College of New Materials and New Energies, Shenzhen Technology University, Shenzhen 518118, China (e-mail: zhangyulong@sztu.edu.cn).

Xinge Guo and Chengkuo Lee are with the Department of Electrical and Computer Engineering, National University of Singapore, Singapore 117576 (e-mail: guoxg@u.nus.edu; elelc@nus.edu.sg).

Yan Lu is with the Institute of Microelectronics, University of Macau (UM), Taipa, Macau, also with the State Key Laboratory of Analog and Mixed-Signal VLSI, University of Macau (UM), Taipa, Macau, and also with the Department of Electrical and Computer Engineering, Faculty of Science and Technology, University of Macau (UM), Taipa, Macau (e-mail: yanlu@um.edu.mo).

Fei Wang is with the School of Microelectronics, SUSTech, Shenzhen 518055, China, and also with the Research Center of Integrated Circuits for Next-Generation Communications, Ministry of Education, SUSTech, Shenzhen 518055, China (e-mail: wangf@sustech.edu.cn).

This article has supplementary material provided by the authors and color versions of one or more figures available at https://doi.org/10.1109/JMEMS.2021.3058766.

Digital Object Identifier 10.1109/JMEMS.2021.3058766

***Index Terms*— Energy harvesting, microelectromechanical systems (MEMS), air damping, perforated electrode.**

I. Introduction

With the rapid development of artificial intelligence, internet of things, and personal health monitoring devices, an increasing number of micro-sensors and actuators are needed in daily life, which are mainly powered by the battery. However, traditional batteries are usually suffering from the difficulties of routine maintenance. Recently, devices or systems with lower power consumption have been developed to extend the lifetime of the battery [1]–[5]. Meanwhile, more and more efforts have been made to employ self-sustainable power sources to replace traditional batteries.

There are many kinds of energy resources around us, such as solar energy, RF energy, thermal energy, wind energy, and mechanical vibration energy. Harvesting energy from the ambient environment to provide power for the low-power devices could be a potential solution to avoid the routine maintenance of the battery. Many self-sustainable energy harvesters have been fabricated, such as solar cell [6], RF energy harvester [7], thermal energy harvester [8], wind energy harvester [9], [10], and vibration energy harvester [11]–[13]. Among these devices, the vibration energy harvester (VEH) has attracted much attention, because the vibration sources are the most widely distributed in human motion, moving vehicles, ocean wave, working machine, and so on.

Generally, there is a moveable component in the VEH, which can sense the external vibration signals and converts them into electricity based on the various energy conversion principles. For the electromagnetic VEH [14]–[18], the energy conversion relies on the Faraday's law of induction. The output power depends on the number of coil turns and the magnetism of magnets in the device. For the piezoelectric VEH [12], [19]–[25], electric energy is generated from the direct conversion of mechanical stress on the piezoelectric materials in the device. In the electrostatic VEH [13], [26]–[35], a variable capacitance structure biased by the pre-charged electret material is utilized to generate power. For triboelectric VEH [9], [36], [37], triboelectric effect is applied to harvest energy from the environment. Among these four VEHs, the electrostatic VEH (e-VEH) exhibits the high output power density and the best IC compatibility [13] which is very suitable for the integrated devices and systems.

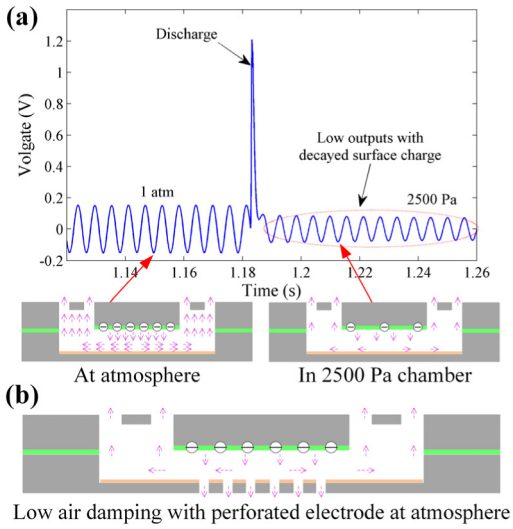

Fig. 1. Electrostatic energy harvester with (a) low outputs with decayed surface charge in vacuum chamber; and (b) low air damping from perforated electrode at atmosphere.

Typically, there are two kinds of e-VEH based on in-plane [38] or out-of-the-plane [39] vibrations. In our previous research, we have reported several e-VEHs based on the out-of-the-plane gap closing scheme, such as the development of the polymer electret for the harsh environment [33], the dual resonant structure for broadband output [34], the sandwich structure for high power output [35]. All of the above-mentioned design approaches can improve the output performance of the device. However, due to the damping force, a relatively large driving acceleration is still required for the device to generate enough power. To solve this problem, we have optimized the air damping of the device and achieved both high normalized power density and broad bandwidth by vacuum packaging [13]. Whereas, for the electrostatic VEH and triboelectric VEH, the surface charge of their electret may suffer from the Paschen discharge under low pressure [40]–[42]. As shown in Figure 1(a), with the decrease of the pressure in the device, a discharge peak suddenly appeared which lead to the deduction of the device's output voltage. Thus, the output power of the low-pressure packaged electrostatic and triboelectric VEH could be obstructed by this phenomenon. In consequence, how to optimize the air damping of the device in atmospheric pressure has been an important issue for the academic community.

In our previous work [43], we have proposed an electrostatic vibration energy harvester with the perforated electrode to decrease the air damping on the moveable proof mass. Compared with the regular electrode, high power output can be achieved with the perforated electrode at low amplitude of external vibration source. However, the perforated electrode plate was manufactured by laser drilling on acrylic plates which is not compatible with IC process. Moreover, some detailed issues are also required for further investigations such as the effect of hole numbers for the induced charge, and the effects of hole numbers, volume ratios for output power. In this work, we propose a design to minimize the air damping at the atmosphere on the moveable proof mass in the e-VEH based on the MEMS process. As shown in Figure 1(b), some through-holes are designed on the fixed plate to control the squeeze-film air damping when the proof mass moves toward the fixed plate. This idea has been well used for many MEMS devices. Ganji *et al.* [44] and Han *et al.* [45] have applied for the perforated electrode in MEMS microphone, which can reduce the chip size and enhance the directional cues by mitigating the squeeze air film damping. Rajavelu *et al.* [46] have employed the perforated diaphragms in piezoresistive MEMS pressure sensor for sensitivity enhancement in gas flow measurement compared with other pressure sensor without perforation. Kamada *et al.* [47] have proposed a capacitive MEMS accelerometer with perforated mass structure, which demonstrates an excellent performance with a low noise floor of less than 30 nG/$\sqrt{}$Hz and a low-power consumption of 20 mW. Li *et al.* [48] have discussed the dynamic performance improving of MEMS sensor by using gas damping structure such as the perforated damping plates and employed the modified Reynolds' equation to analyze the gas damping effects of perforated plates for small amplitude vibration. Herein, it is the first time to apply the perforated electrode in a MEMS e-VEH. We will discuss the effect of the holes on the output power of the e-VEH from the finite element method (FEM) simulation and the experiment results below in this paper.

TABLE I
PARAMETERS OF THE PERFORATED E-VEH IN FEM SIMULATION

Parameters	Value	Description
w (μm)	200	Beam width
l (mm)	7	Beam length
h_1 (μm)	60	Beam thickness
S_0 (mm^2)	90.25	Surface area of the square proof mass
h_2 (μm)	500	Thickness of proof mass
g (μm)	340	Initial gap between the parallel plates
H (μm)	100	Depth of holes
S_{hole}/S_0	5.01%, 11.3%, 20.05%, 45.11%	Volume ratio of the holes
U (V)	-450	Surface potential of the proof mass

II. DESIGN AND MODELING

As shown in Figure 2(a), the perforated e-VEH is designed based on the out-of-the-plane gap closing scheme. Through-holes are distributed on the bottom fixed electrode plate. Hence, when the proof mass is driven to move toward the fixed plate, the air between the proof mass and the bottom plate can be extruded through these holes. The air damping on the proof mass will be efficiently reduced. Figure 2(b) shows the layout of the top spring-mass structure, which is designed as a square proof mass suspended by a fixed frame through four beams. We have simulated the air damping force on the proof mass and the induced surface charge on the perforated electrode using finite element modeling method (COMSOL).

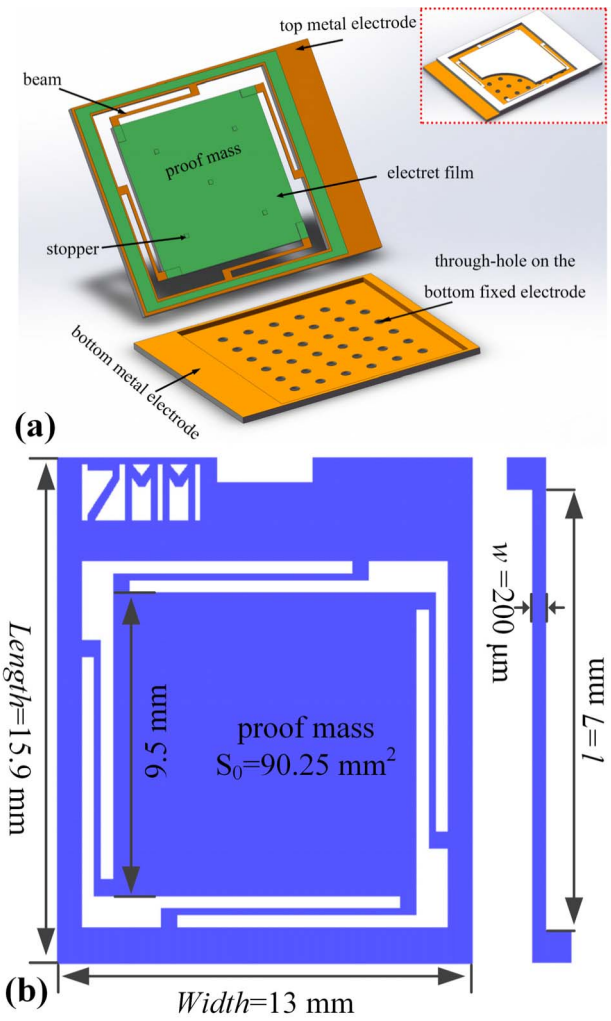

Fig. 2. (a) 3D schematic of the perforated electrostatic energy harvester. (b) Layout of the resonant structure.

Table I lists the structural parameters of the perforated device in the following simulations. To simplify the calculation, the geometric model of the spring-mass is divided into four parts symmetrically. First, the resonant frequency of the device and the stress distribution in the beam are calculated as shown in Supplementary Figure S1. The resonant frequency (the first order of out-of-plane vibration mode) of this spring-mass structure is calculated as 132.46 Hz, and the maximum stress across the beam is 203 MPa when the displacement of the proof mass is defined as 340 μm, which is lower than the fracture limit of single-crystal silicon (up to ~7 GPa [49]). Hence, the beam can bear the stress during vibration.

A. Squeeze-Film Air Damping on the Proof Mass

In this out-of-the-plane e-VEH, the air damping on the moveable proof mass mainly comes from squeeze-film air damping. Referring to the Reynolds' equation, Bao *et al.* [50] have proposed a model to describe the squeeze-film air damping for perforated plate. In this paper, based on the Bao's model, the bottom fixed plate with a square area of 90.25 mm^2 is divided into densely arranged equal circular cells according

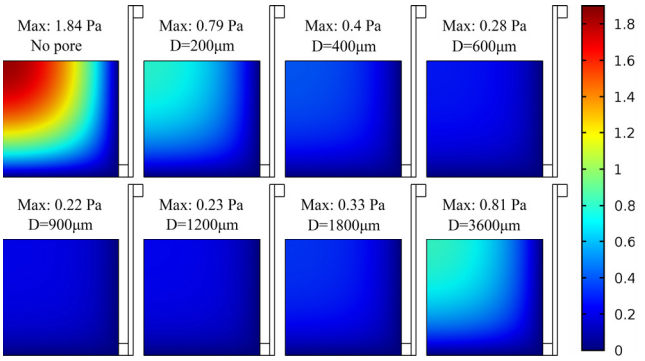

Fig. 3. FEM simulated squeeze-film air damping pressure on the proof mass under the velocity of −0.05 m/s at the volume ratio of the holes of 11.3%.

to the number of holes. The holes are allocated in the center of these circular cells. So, the modified Reynolds' equation for the squeeze-film air damping of the hole plate is written as

$$\frac{\partial^2 \mathrm{P}}{\partial x^2} + \frac{\partial^2 \mathrm{P}}{\partial y^2} - \frac{3\beta^2 r_0^2}{2h^3 H_{eff}} \frac{1}{\eta(\beta)} P = \frac{12\mu}{h^3} \frac{\partial h}{\partial t} \tag{1}$$

$$\mathrm{H}_{eff} = \mathrm{H} + \frac{3\pi r_0}{8} \tag{2}$$

$$\eta(\beta) = 1 + \frac{3r_0^4 k(\beta)}{16 H h^3} \tag{3}$$

$$k(\beta) = 4\beta^2 - \beta^4 - 4\ln\beta - 3 \tag{4}$$

$$\beta = \frac{r_0}{r_c} \tag{5}$$

where μ is the coefficient of viscosity of air (1.81×10^{-5} Pa · sec); H and h represent the depth of the hole and the distance from the proof mass to the perforated plate, respectively; r_0 and r_c stand for the radiuses of the holes and the circular cells. In COMSOL, we could use the finite element method to solve the modified Reynolds' equation, and the damping pressure distribution on the surface of proof mass at different velocities can be obtained. The damping force on the whole proof mass is therefore acquired by integrating the damping pressure on the surface of the proof mass.

Figure 3 shows the squeeze-film air damping pressure on the proof mass under the velocity of −0.05 m/s when the volume ratio of the holes is 11.3%. After perforating on the bottom electrode plate, the maximum air damping pressure is obviously reduced. We can see the damping pressure on the proof mass is well controlled down to 12-22% of the original value when the hole diameter is increased from 400 μm to 1800 μm. For comparison, the pressure distributions on the proof mass are simulated with other volume ratios of the holes, such as 5.01%, 20.05% and 45.11%.

As demonstrated in Figure 4, with the increase of the hole diameter, the air damping force decreases first and then increases under the same volume ratio of holes. When the hole diameter is decreased, the air between two plates cannot penetrate through the hole timely during vibration because of the pressure build-up in the hole. Therefore, increasing the hole diameter can reduce the damping force. With the increase of the hole diameter, the number of the hole will decrease at

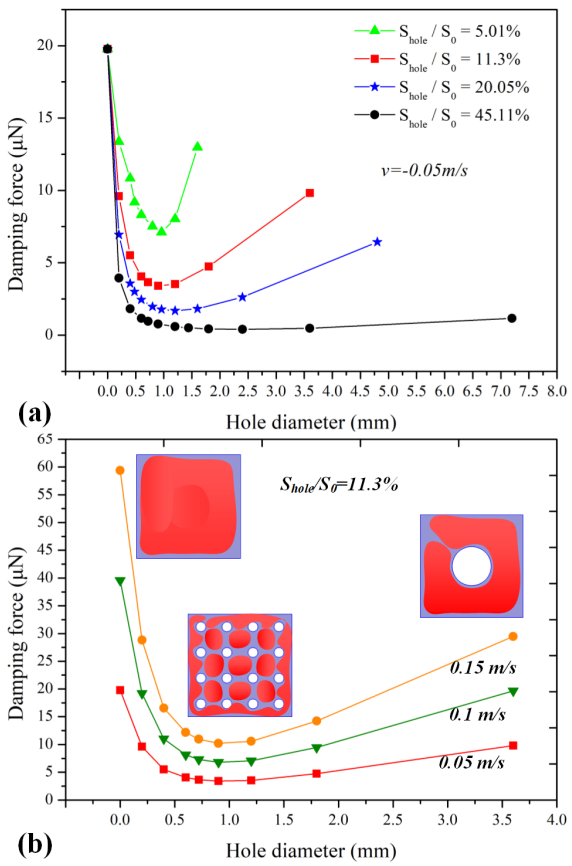

Fig. 4. FEM simulated squeeze-film air damping force on the proof mass under (a) different volume ratio of the holes, and (b) different velocity and the analysis diagram of the effect of holes on the air film.

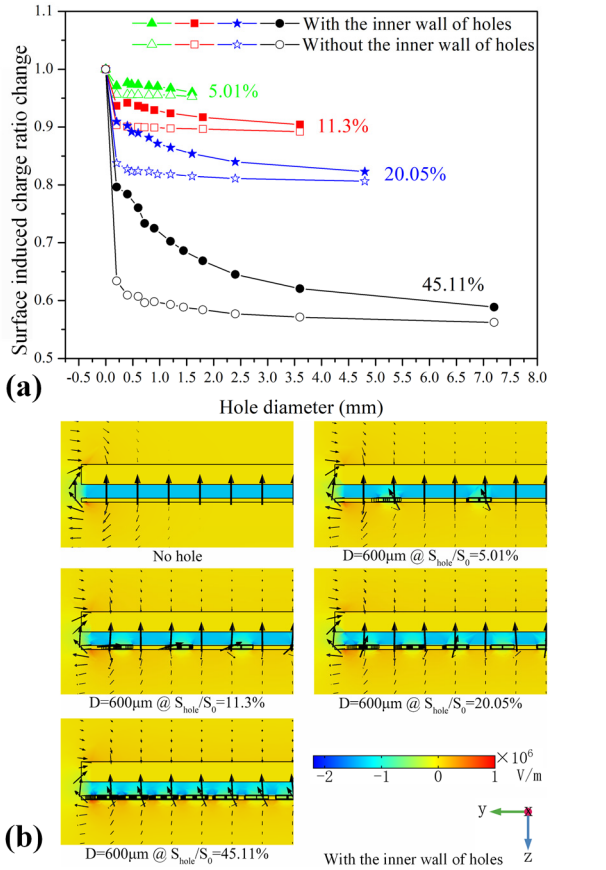

Fig. 5. FEM simulated (a) surface induced charge change with and without the inner wall of holes, and (b) electric field between the perforated electrode and the proof mass.

the same time. If the hole diameter is too big at the same volume ratio, however, the number of holes will decrease dramatically, which leads to air compression in the relatively large area. Hence, the damping force will increase again. For vibration velocity from 0.05 m/s to 0.15 m/s, we have found that the air damping effect could be optimized with hole diameter from 400 μm to 1200 μm, as shown in Figure 4(b).

B. Surface Induced Charge on the Perforated Electrode

The core structure in our electrostatic vibration energy harvester is a variable capacitor with parallel-plate. Once the electret on the proof mass is charged, induced charges will be generated on the surface of the bottom electrode plate when the electret approaches. Driven by the external vibration, the proof mass moves up and down, and the induced charge will flow between the two electrodes, which generates the output current. Perforating on the bottom fixed plate may cause the sacrifice of the surface electrode. Thus, the effect of the hole on the induced charge is an important issue for the output performance of the perforated e-VEH.

The induced surface charge of the perforated electrode can be simulated when the surface potential of the electret layer is set to −450 V. Herein, we calculate the change of the induced charge with and without the inner wall of holes as shown in Figure 5(a). It indicates that the inner wall of holes can compensate the charge loss due to the reduced surface area of the bottom electrode. Furthermore, more perforated holes with larger the inner wall area, could bring the better compensation. It can also be noticed from the Figure 5(a) that the surface induced charge keeps above 80% of the original value after perforating when the volume ratio of holes is less than 20.05%. Figure 5(b) shows the electric field distributions between the proof mass and the perforated electrode with the hole diameter of 600 μm at the different volume ratios. Due to the edge effect caused by the holes, the electric field between the two parallel-plates becomes slightly non-uniform, and the fringe effect could be noticed as the electric field lines expand from the area between the two plates to the outer space.

Based on the simulations above, optimal design with a hole diameter of 400 μm is chosen and more simulations are performed to study the effect of hole numbers. As shown in Figure 6(a), more than 84.5% of the induced surface charge can be maintained when the hole number is no more than 225. A linear relationship between the reduction of the induced charge and the holes' number is achieved based on the simulation. On the other hand, the change in air damping force is almost exponential to the number of holes as demonstrated in Figure 6(b). Once the number of holes increases from 0 to 100, the damping force decreases dramatically, and the air damping force on the proof mass is only 23.9% of the original value when the hole number is 100. Therefore, the output

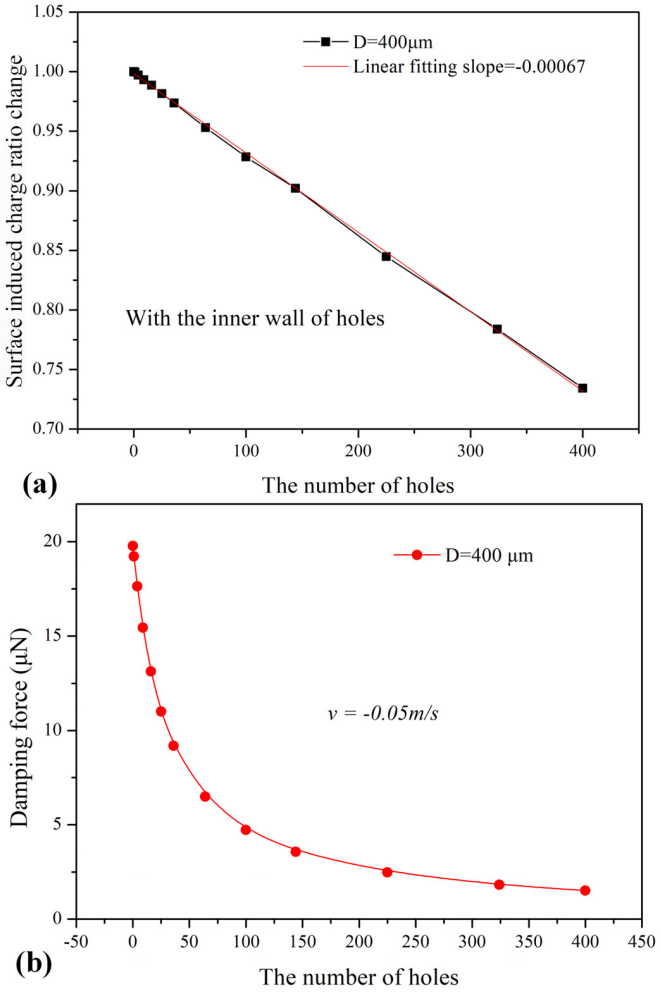

Fig. 6. FEM simulated (a) surface induced charge change, and (b) squeeze-film air damping force of the proof mass at the hole diameter of 400 μm.

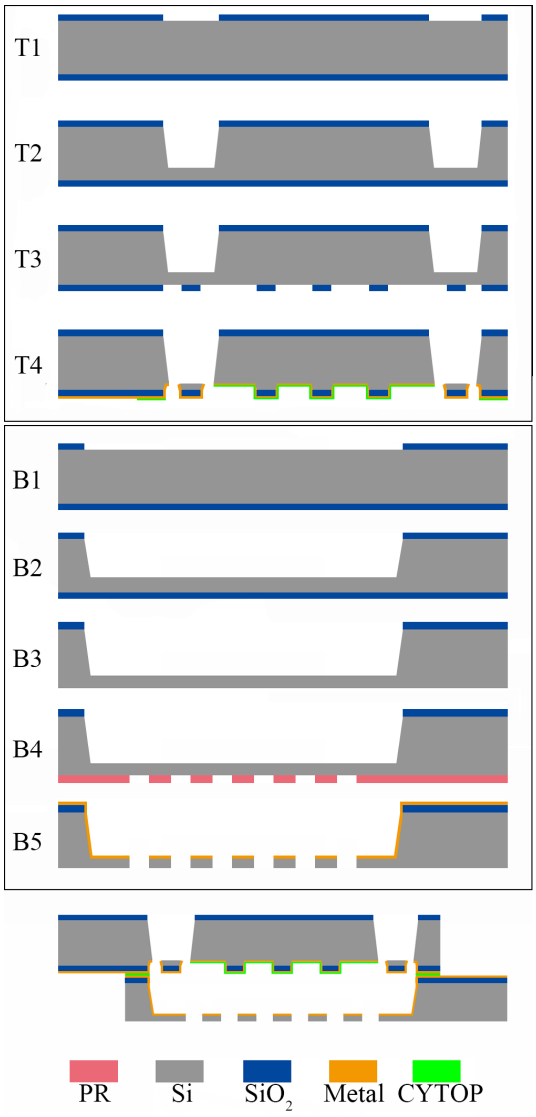

Fig. 7. Process flow for the resonant structure (T1-T4) and perforated structure (B1-B5).

power of the device could be promoted by perforating on the plate.

III. Experiment

There are two components in the perforated e-VEH, the top resonant structure with proof-mass, and the bottom perforated fixed plate. We have fabricated several perforated e-VEHs with different hole diameters to find out the effect of the holes. The fabrication processes are the standard MEMS techniques based on the 4-inch silicon wafer with a thickness of 500 μm. In this section, we will describe the device fabrication process and experiment setup, and then discuss the experimental results in detail below.

A. Device Fabrication

Figure 7 demonstrates the fabrication process of the resonant structure from T1 to T4. First, one side of the double-oxidized silicon wafer is patterned by the photolithography and buffered oxide etchant (BOE) to form the etch mask for the proof mass. Then, KOH solution is used to form the 3D structure of the proof mass. Afterwards, photolithography and the reactive ion etching (RIE) technology are applied to pattern the other side of the wafer. The basis of beam and stopper structures are therefore obtained. Finally, the wafer is etched again from both sides in the KOH solution to release the beam structures. The metal electrode and the electret layer are sequentially coated on the surface of the proof mass, and the electret is charged by the corona charging method.

B1 to B5 depict the fabrication process of the perforated plate which is also based on a double oxidized silicon wafer. Initially, photolithography, BOE etching, and KOH etching, in turn, are employed to form a square cavity on the one side of the silicon wafer with an etch depth of 280 μm. Then, the SiO_2 layer on the other side of the wafer is removed by RIE, and the KOH solution is used again to etch the silicon from both sides to form the final cavity with the depth of 340 μm and to thinner the wafer to a thickness of 440 μm. After the fabrication of the cavity, the circular holes are patterned from the bottom outside of the cavity by photolithography. Finally, we apply the deep RIE technology to perforate the cavity to form the array of holes, and the metal layer is coated on the

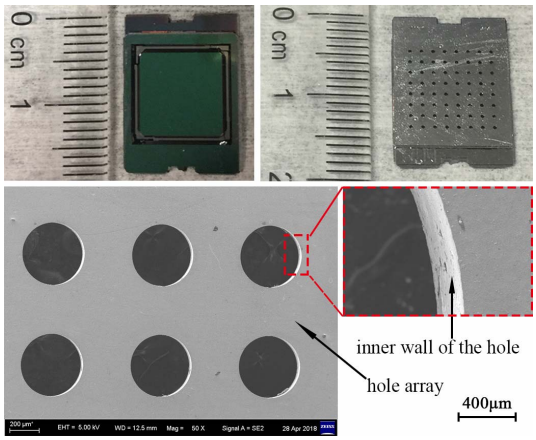

Fig. 8. The final device after bonding, and the SEM image of the hole after DRIE.

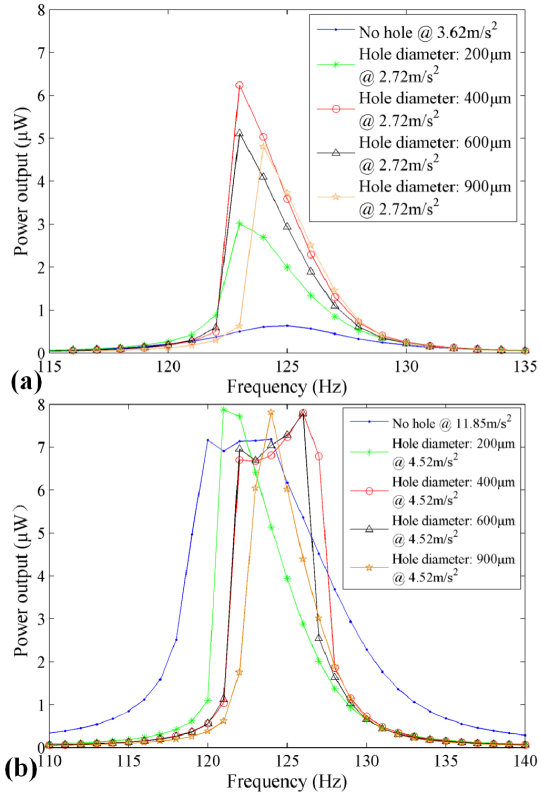

Fig. 9. Power output of the perforated device with different hole size at the volume ratio of the holes of 11.3%. (a) Low acceleration of (3.62 m/s^2 for device without hole and 2.72 m/s^2 for perforated device). (b) High acceleration of (11.85 m/s^2 for device without hole and 4.52 m/s^2 for perforated device).

top surface of the cavity by sputtering. Figure 8 shows the SEM image of the holes with a diameter of 400 μm.

After the fabrication of the two plates, they are bonded together to form the whole perforated e-VEH. As demonstrated in Figure 8, the overall volume of the device is about 0.22 cm^3.

B. Output Performance With Constant Volume Ratio But Different Hole Diameters

In this part, we will investigate the influence of the perforated electrode on the power output of the e-VEH. A series of perforated electrode plates with various hole diameters at the same volume ratio of holes (11.3%) are selected. The surface potential of the electret on the proof mass is about −450 V after charging. Similar to our previous work [51], Figure S2(a) in Supplementary material demonstrates the schematic of the measurement system, where the device is fixed on the shaker to mimic the vibrations in ambient environment. Herein, the devices are all driven by the sinusoidal vibration signals which are generated by a signal generator (Brüel&Kjær, LAN-XI 3160) and a power amplifier (Brüel&Kjær, 2719). As shown in Supplementary Figure S2(b), the optimal load resistances of these perforated devices are measured first. The result indicates that the match resistance maintains the same at 28 MΩ despite of the variation of hole diameters. Hence, the output powers of all the devices will be evaluated under this load resistance.

As depicted in Figure 9, the frequency response of the perforated device is investigated at different vibration accelerations. At an acceleration amplitude of 2.72 m/s^2, the device with hole diameter of 400 μm exhibits the best output performance, and the maximum power of the perforated device is about 9.8 times than that of the device without holes, which proves that the perforation can promote the performance of energy harvester at low driving acceleration. This is because the holes can reduce

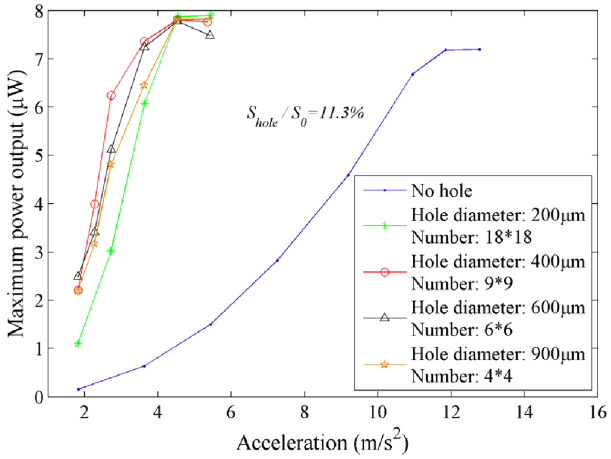

Fig. 10. The maximum power outputs of the perforated devices with different hole size at the constant volume ratio of the holes of 11.3%.

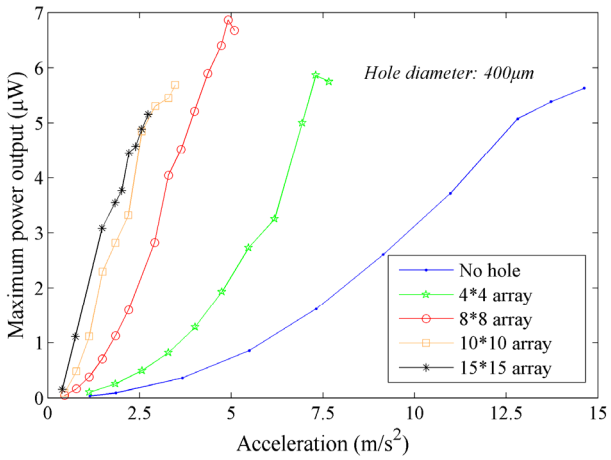

Fig. 11. The maximum power output of the perforated device with hole diameter of 400 μm at different number of holes.

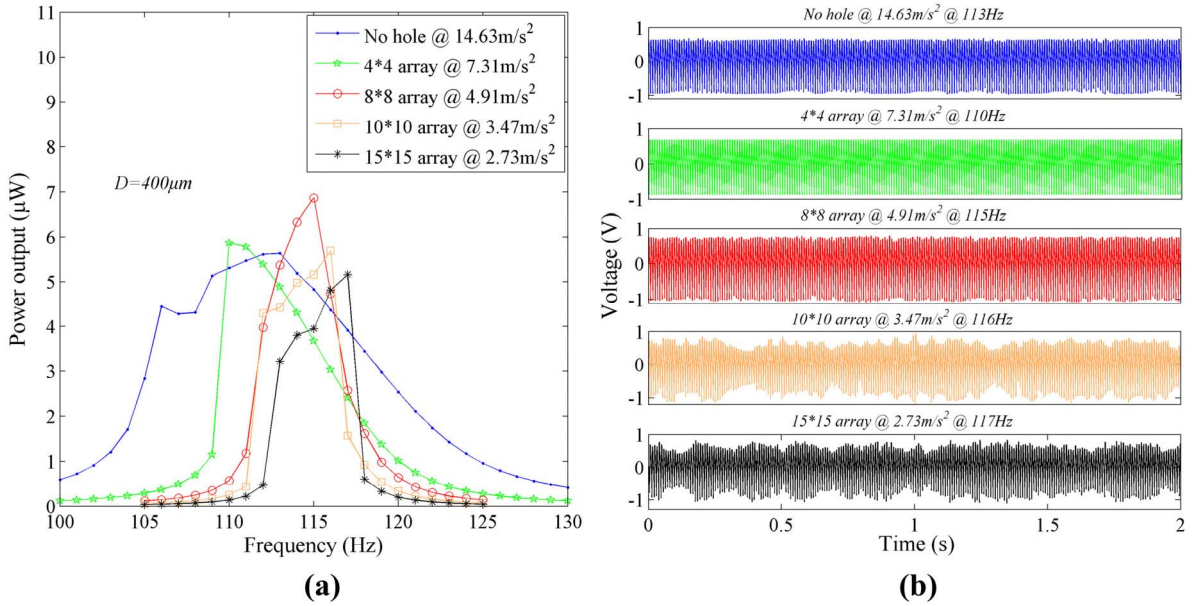

Fig. 12. (a) The power output of the perforated device with hole diameter of 400 μm when the displacement of the proof mass reaches the maximum vibration amplitude driving by different acceleration. (b) The voltage output on the load resistance of 1 MΩ at the resonant frequency.

the squeeze-film air damping force on the proof mass, which means the proof mass can move closer to the bottom plate under the same driving acceleration. Therefore, a higher output power could be generated as the variation of induced charge on the perforated electrode is more substantial. Furthermore, we have also studied the performance of the devices under a relatively higher driving acceleration. As shown in Figure 9(b), when the acceleration continues to increase, the proof mass will move to the limited displacement (It is less than 340 μm considering the limitation of squeeze-film air damping.), where the output power reaches the upper limit. Herein, for the perforated device, it only requires a driving acceleration of 4.52 m/s^2 to reach the maximum vibration amplitude, while for the unperforated device, a large driving acceleration of 11.85 m/s^2 is needed which is about 2.6 times larger than the former. It should also be noticed that, at the limit position, the maximum power outputs of all the perforated devices are a little bit larger than the unperforated device.

Figure 10 exhibits the maximum power outputs of the perforated devices with the various hole diameters at a constant volume ratio of holes of 11.3% at the resonant frequency. When the driving acceleration is insufficient for the device to reach the limit position, the device with the hole diameter of 400 μm shows the highest output power at the same driving accelerations. The reason is that the air damping force on the proof mass in this device is smaller than others, which makes the displacement of the proof mass larger. Moreover, this phenomenon is similar to the relationship between the air damping force and the hole diameter as mentioned in FEM simulation results before.

C. Output Performance With Increasing Volume Ratio by Different Hole Numbers

Based on the results above, it could be noticed that the device with hole diameter of 400 μm exhibits outstanding performance under the constant volume ratio of 11.3%. Therefore, in this part, we will tune the volume ratio of the device by increasing the number of the holes at the same diameter of 400 μm to further study the effect of hole number on the output performance of the perforated e-VEH. Similarly, the optimal load resistances of these perforated devices with different hole numbers are tested first, and their match resistances are still maintained at 28 MΩ according to the experiment results. Then, we have measured the maximum output power of these devices under the resonant frequency as demonstrated in Figure 11. According to the results, the output power increases with the increase of the hole number at the low driving acceleration. However, with the increase of the driving acceleration, the device with an 8×8 holes array shows the best output power among these devices.

Figure 12(a) depicts the power outputs of the devices with different hole numbers at the limited displacement when driven at different accelerations. It could be noticed that the more the hole perforated on the device, the smaller the driving acceleration is required for the proof mass to move to the limited displacement. Whereas, there is a little bit of difference in the maximum power at the limited position. Initially, the power output increases with the increase of the hole number. It is because the maximum displacement of the proof mass in the perforated device with more holes is closer to 340 μm when the squeeze-film air damping is optimized. However, the output power cannot be unlimitedly promoted by perforating more holes on the plate. When the number of holes continues to increase to more than 100, the maximum power can decrease a little. Similar phenomenon could also be noticed in Figure 12(b), where the output voltage of the device becomes unstable when the number of holes on the plate is more than 100. This could be explained as the smaller air damping force on the device with more holes can cause stronger collision between the proof mass and the

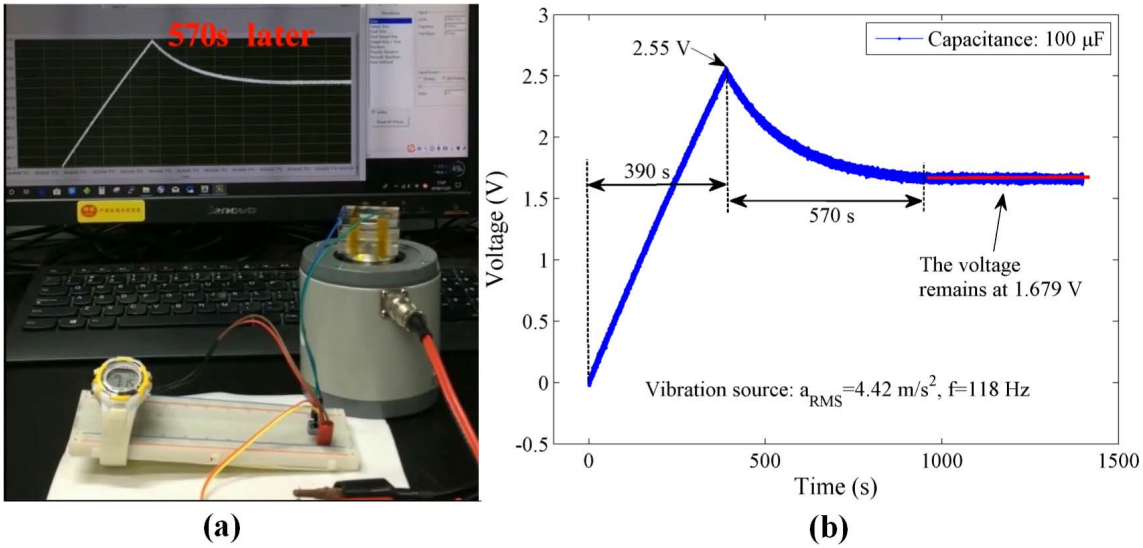

Fig. 13. (a) An electronic watch powered by the perforated energy harvester with 8*8 holes array. (b) The voltage on the capacitor (in parallel to the electronic watch) can maintain at about 1.68 V after 570 s.

fixed plate under a certain driving acceleration, and the violent collision between the moveable proof mass and the fixed plate leads to the unstable motion of the proof mass. Therefore, the calculated root mean square power is lower than that of the steady state. Moreover, the frequency response and the displacement waveform of the device with different holes at the driving acceleration of 1.84 m/s^2 could be found in Supplementary Figure S3.

D. Application of the Perforated Energy Harvester

We have applied the perforated energy harvester with 8×8 holes array to provide power for an electronic watch. Figure 13(a) depicts the image of the experiment. Similar to the above-mentioned testing condition, the perforated device was mounted on the shaker to harvest energy from vibration, and the shaker was excited by a 118 Hz sinusoidal signal with a low acceleration of 4.42 m/s^2. The output voltage of the device was rectified to charge a 100 μF capacitor. The voltage of the capacitor was charged to 2.55 V after 390 s as Figure 13(b) demonstrated. At this time, the electronic watch was connected to the capacitor and lighted up. A slight drop of the voltage on the capacitor was noticed in the following 570 s. In spite of this, the voltage remains at about 1.68 V afterwards, proving that the device could provide enough power for self-powered electronics even under the vibration with low acceleration. The video of this experiment could be obtained in Supplementary Video S1.

IV. Conclusion

This paper presents an electrostatic vibration energy harvester with the perforated electrode. Through-holes are designed on the fixed plate of the e-VEH to reduce the squeeze-film air damping between the moveable proof mass and the fixed plate. In the FEM simulation, we have found that the damping force on the proof mass in the perforated device decreases dramatically, while the surface induced charge on the perforated electrode could be well maintained. We have fabricated the device with MEMS technology, and the effect of the hole diameters is investigated in detail. The experiment results have further proved that the device with perforated plate can generate more power than the device without holes from the same low amplitude of external vibration. Finally, we have applied the perforated device to provide power for an electronic watch when driving by a low acceleration of 4.42 m/s^2. The voltage between the watch can maintain at about 1.68 V which proves a promising application for self-powered electronics.

Acknowledgment

The authors would like to thank the technical support from the Materials Characterization and Preparation Center, Southern University of Science and Technology.

References

[1] T. Itoh, "Ultra low power wireless sensor nodes for expanding application of the Internet of Things," in *Proc. IEEE CPMT Symp. Jpn. (ICSJ)*, Nov. 2016, pp. 74–75, doi: 10.1109/ICSJ.2016.7801319.

[2] J. M. Lambrecht and R. F. Kirsch, "Miniature low-power inertial sensors: Promising technology for implantable motion capture systems," *IEEE Trans. Neural Syst. Rehabil. Eng.*, vol. 22, no. 6, pp. 1138–1147, Nov. 2014, doi: 10.1109/TNSRE.2014.2324825.

[3] J.-H. Kim, A. Mirzaei, H. W. Kim, and S. S. Kim, "Low power-consumption CO gas sensors based on Au-functionalized SnO_2-ZnO core-shell nanowires," *Sens. Actuators B, Chem.*, vol. 267, pp. 597–607, Aug. 2018, doi: 10.1016/j.snb.2018.04.079.

[4] Y. Pu *et al.*, "Blackghost: An ultra-low-power all-in-one 28 nm CMOS SoC for Internet-of-Things," in *Proc. IEEE Symp. Low-Power High-Speed Chips (COOL CHIPS)*, Apr. 2017, pp. 1–3, doi: 10.1109/CoolChips.2017.7946384.

[5] G. Niu, C. Zhao, H. Gong, Z. Yang, X. Leng, and F. Wang, "NiO nanoparticle-decorated SnO_2 nanosheets for ethanol sensing with enhanced moisture resistance," *Microsystems Nanoeng.*, vol. 5, no. 1, p. 21, Dec. 2019, doi: 10.1038/s41378-019-0060-7.

[6] Q. Tang, H. Zhang, B. He, and P. Yang, "An all-weather solar cell that can harvest energy from sunlight and rain," *Nano Energy*, vol. 30, pp. 818–824, Dec. 2016, doi: 10.1016/j.nanoen.2016.09.014.

[7] Y. Lu *et al.*, "A wide input range dual-path CMOS rectifier for RF energy harvesting," *IEEE Trans. Circuits Syst. II, Exp. Briefs*, vol. 64, no. 2, pp. 166–170, Feb. 2017, doi: 10.1109/TCSII.2016.2554778.

[8] J. Yan, X. Liao, D. Yan, and Y. Chen, "Review of micro thermoelectric generator," *J. Microelectromech. Syst.*, vol. 27, no. 1, pp. 1–18, Feb. 2018, doi: 10.1109/JMEMS.2017.2782748.

[9] Y. Wu, Y. Hu, Z. Huang, C. Lee, and F. Wang, "Electret-material enhanced triboelectric energy harvesting from air flow for self-powered wireless temperature sensor network," *Sens. Actuators A, Phys.*, vol. 271, pp. 364–372, Mar. 2018, doi: 10.1016/j.sna.2017.12.067.

[10] K. Yang, J. Wang, and D. Yurchenko, "A double-beam piezo-magneto-elastic wind energy harvester for improving the galloping-based energy harvesting," *Appl. Phys. Lett.*, vol. 115, no. 19, Nov. 2019, Art. no. 193901, doi: 10.1063/1.5126476.

[11] X. He, Q. Wen, Y. Sun, and Z. Wen, "A low-frequency piezoelectric-electromagnetic-triboelectric hybrid broadband vibration energy harvester," *Nano Energy*, vol. 40, pp. 300–307, Oct. 2017, doi: 10.1016/j.nanoen.2017.08.024.

[12] Q. Tang and X. Li, "Two-stage wideband energy harvester driven by multimode coupled vibration," *IEEE/ASME Trans. Mechatronics*, vol. 20, no. 1, pp. 115–121, Feb. 2015, doi: 10.1109/TMECH.2013.2296776.

[13] Y. Zhang, T. Wang, A. Luo, Y. Hu, X. Li, and F. Wang, "Micro electrostatic energy harvester with both broad bandwidth and high normalized power density," *Appl. Energy*, vol. 212, pp. 362–371, Feb. 2018, doi: 10.1016/j.apenergy.2017.12.053.

[14] A. Luo *et al.*, "An inertial rotary energy harvester for vibrations at ultra-low frequency with high energy conversion efficiency," *Appl. Energy*, vol. 279, Dec. 2020, Art. no. 115762, doi: 10.1016/j.apenergy.2020.115762.

[15] Q. Zhang and E. S. Kim, "Vibration energy harvesting based on magnet and coil arrays for watt-level handheld power source," *Proc. IEEE*, vol. 102, no. 11, pp. 1747–1761, Nov. 2014, doi: 10.1109/JPROC.2014.2358995.

[16] X. Liu, J. Qiu, H. Chen, X. Xu, Y. Wen, and P. Li, "Design and optimization of an electromagnetic vibration energy harvester using dual Halbach arrays," *IEEE Trans. Magn.*, vol. 51, no. 11, pp. 1–4, Nov. 2015, doi: 10.1109/TMAG.2015.2437892.

[17] M. A. Halim, R. Rantz, Q. Zhang, L. Gu, K. Yang, and S. Roundy, "An electromagnetic rotational energy harvester using sprung eccentric rotor, driven by pseudo-walking motion," *Appl. Energy*, vol. 217, pp. 66–74, May 2018, doi: 10.1016/j.apenergy.2018.02.093.

[18] Y. Zhang, A. Luo, Y. Wang, X. Dai, Y. Lu, and F. Wang, "Rotational electromagnetic energy harvester for human motion application at low frequency," *Appl. Phys. Lett.*, vol. 116, no. 5, Feb. 2020, Art. no. 053902, doi: 10.1063/1.5142575.

[19] L. S. Mendonca, L. T. Martins, M. Radecker, F. E. Bisogno, and D. Killat, "Normalized modeling of piezoelectric energy harvester based on equivalence transformation and unit-less parameters," *J. Microelectromech. Syst.*, vol. 28, no. 4, pp. 666–677, Aug. 2019, doi: 10.1109/JMEMS.2019.2921649.

[20] M. T. Todaro *et al.*, "Piezoelectric MEMS vibrational energy harvesters: Advances and outlook," *Microelectron. Eng.*, vols. 183–184, pp. 23–36, Nov. 2017, doi: 10.1016/j.mee.2017.10.005.

[21] S. Li, Z. Peng, A. Zhang, and F. Wang, "Dual resonant structure for energy harvesting from random vibration sources at low frequency," *AIP Adv.*, vol. 6, no. 1, Jan. 2016, Art. no. 015019, doi: 10.1063/1.4941353.

[22] S. Du *et al.*, "A new electrode design method in piezoelectric vibration energy harvesters to maximize output power," *Sens. Actuators A, Phys.*, vol. 263, pp. 693–701, Aug. 2017, doi: 10.1016/j.sna.2017.06.026.

[23] X. He, Q. Wen, Z. Lu, Z. Shang, and Z. Wen, "A micro-electromechanical systems based vibration energy harvester with aluminum nitride piezoelectric thin film deposited by pulsed direct-current magnetron sputtering," *Appl. Energy*, vol. 228, pp. 881–890, Oct. 2018, doi: 10.1016/j.apenergy.2018.07.001.

[24] Y. Tian, G. Li, Z. Yi, J. Liu, and B. Yang, "A low-frequency MEMS piezoelectric energy harvester with a rectangular hole based on bulk PZT film," *J. Phys. Chem. Solids*, vol. 117, pp. 21–27, Jun. 2018, doi: 10.1016/j.jpcs.2018.02.024.

[25] S. Nabavi and L. Zhang, "T-shaped piezoelectric structure for high-performance MEMS vibration energy harvesting," *J. Microelectromech. Syst.*, vol. 28, no. 6, pp. 1100–1112, Dec. 2019, doi: 10.1109/JMEMS.2019.2942291.

[26] U. Bartsch, J. Gaspar, and O. Paul, "A 2D electret-based resonant micro energy harvester," in *Proc. IEEE 22nd Int. Conf. Micro Electro Mech. Syst.*, Jan. 2009, pp. 1043–1046, doi: 10.1109/MEMSYS.2009.4805565.

[27] Y. Suzuki, "Recent progress in MEMS electret generator for energy harvesting," *IEEJ Trans. Electr. Electron. Eng.*, vol. 6, no. 2, pp. 101–111, Mar. 2011, doi: 10.1002/tee.20631.

[28] A. Crovetto, F. Wang, and O. Hansen, "An electret-based energy harvesting device with a wafer-level fabrication process," *J. Micromech. Microeng.*, vol. 23, no. 11, Oct. 2013, Art. no. 114010, doi: 10.1088/0960-1317/23/11/114010.

[29] K. Tao, S. W. Lye, J. Miao, L. Tang, and X. Hu, "Out-of-plane electret-based MEMS energy harvester with the combined nonlinear effect from electrostatic force and a mechanical elastic stopper," *J. Micromech. Microeng.*, vol. 25, no. 10, Sep. 2015, Art. no. 104014, doi: 10.1088/0960-1317/25/10/104014.

[30] Y. Lu, F. Cottone, S. Boisseau, F. Marty, P. Basset, and D. Galayko, "Low-frequency and ultra-wideband MEMS electrostatic vibration energy harvester powering an autonomous wireless temperature sensor node," in *Proc. IEEE 29th Int. Conf. Micro Electro Mech. Syst. (MEMS)*, Jan. 2016, pp. 33–36, doi: 10.1109/MEMSYS.2016.7421550.

[31] K. Tao, L. Tang, J. Wu, S. W. Lye, H. Chang, and J. Miao, "Investigation of multimodal electret-based MEMS energy harvester with impact-induced nonlinearity," *J. Microelectromech. Syst.*, vol. 27, no. 2, pp. 276–288, Apr. 2018, doi: 10.1109/JMEMS.2018.2792686.

[32] M. Ghavami, S. Azizi, and M. R. Ghazavi, "On the dynamics of a capacitive electret-based micro-cantilever for energy harvesting," *Energy*, vol. 153, pp. 967–976, Jun. 2018, doi: 10.1016/j.energy.2018.04.034.

[33] Y. Xu *et al.*, "Spray coating of polymer electret with polystyrene nanoparticles for electrostatic energy harvesting," *Micro Nano Lett.*, vol. 11, no. 10, pp. 640–644, Oct. 2016, doi: 10.1049/mnl.2016.0336.

[34] Y. Zhang, A. Luo, Y. Xu, T. Wang, and F. Wang, "Wideband MEMS electrostatic energy harvester with dual resonant structure," in *Proc. IEEE SENSORS*, Orlando, FL, USA, Oct. 2016, pp. 1–3, doi: 10.1109/ICSENS.2016.7808945.

[35] Y. Zhang, Y. Hu, X. Guo, and F. Wang, "Micro energy harvester with dual electrets on sandwich structure optimized by air damping control for wireless sensor network application," *IEEE Access*, vol. 6, pp. 26779–26788, 2018, doi: 10.1109/ACCESS.2018.2836381.

[36] Y. Zi, H. Guo, Z. Wen, M.-H. Yeh, C. Hu, and Z. L. Wang, "Harvesting low-frequency (<5 Hz) irregular mechanical energy: A possible killer application of triboelectric nanogenerator," *ACS Nano*, vol. 10, no. 4, pp. 4797–4805, Apr. 2016, doi: 10.1021/acsnano.6b01569.

[37] S. A. Shankaregowda *et al.*, "Single-electrode triboelectric nanogenerator based on economical graphite coated paper for harvesting waste environmental energy," *Nano Energy*, vol. 66, Dec. 2019, Art. no. 104141, doi: 10.1016/j.nanoen.2019.104141.

[38] Y. Suzuki, D. Miki, M. Edamoto, and M. Honzumi, "A MEMS electret generator with electrostatic levitation for vibration-driven energy-harvesting applications," *J. Micromech. Microeng.*, vol. 20, no. 10, Sep. 2010, Art. no. 104002, doi: 10.1088/0960-1317/20/10/104002.

[39] F. Wang and O. Hansen, "Electrostatic energy harvesting device with out-of-the-plane gap closing scheme," *Sens. Actuators A, Phys.*, vol. 211, pp. 131–137, May 2014, doi: 10.1016/j.sna.2014.02.027.

[40] A. Viraneva, T. Yovcheva, and G. Mekishev, "Pressure effect on the polymer electret films," *IEEE Trans. Dielectr. Electr. Insul.*, vol. 20, no. 5, pp. 1882–1886, Oct. 2013, doi: 10.1109/TDEI.2013.6633720.

[41] S. Lv *et al.*, "Gas-enhanced triboelectric nanogenerator based on fully-enclosed structure for energy harvesting and sensing," *Nano Energy*, vol. 55, pp. 463–469, Jan. 2019, doi: 10.1016/j.nanoen.2018.11.022.

[42] Y. Zhang *et al.*, "Ferroelectret materials and devices for energy harvesting applications," *Nano Energy*, vol. 57, pp. 118–140, Mar. 2019, doi: 10.1016/j.nanoen.2018.12.040.

[43] Y. Zhang, X. Quo, and F. Wang, "Perforated electrode for performance optimization of electrostatic energy harvester," in *Proc. IEEE Micro Electro Mech. Syst. (MEMS)*, Belfast, U.K., Jan. 2018, pp. 612–615, doi: 10.1109/MEMSYS.2018.8346628.

[44] B. A. Ganji and B. Y. Majlis, "Deposition and etching of diaphragm and sacrificial layer in novel MEMS capacitive microphone structure," in *Proc. IEEE Int. Conf. Semiconductor Electron.*, Nov. 2008, pp. 232–238, doi: 10.1109/SMELEC.2008.4770314.

[45] S. Han, A. Ishfaque, P. Phamduy, and B. Kim, "Effect of squeeze air film damping on diffraction grating based bio-inspired MEMS directional microphone," *Microsyst. Technol.*, vol. 26, no. 4, pp. 1203–1212, Apr. 2020, doi: 10.1007/s00542-019-04650-6.

[46] M. Rajavelu, D. Sivakumar, R. J. Daniel, and K. Sumangala, "Perforated diaphragms employed piezoresistive MEMS pressure sensor for sensitivity enhancement in gas flow measurement," *Flow Meas. Instrum.*, vol. 35, pp. 63–75, Mar. 2014, doi: 10.1016/j.flowmeasinst.2013.12.004.

[47] Y. Kamada, A. Isobe, T. Oshima, Y. Furubayashi, T. Ido, and T. Sekiguchi, "Capacitive MEMS accelerometer with perforated and electrically separated mass structure for low noise and low power," *J. Microelectromech. Syst.*, vol. 28, no. 3, pp. 401–408, Jun. 2019, doi: 10.1109/JMEMS.2019.2903349.

[48] L. Li, R. Zhu, Z. Zhou, and J. Ren, "Dynamic performance improving of MEMS sensor by gas damping structure," in *Proc. IEEE Int. Symp. Knowl. Acquisition Modeling Workshop*, Dec. 2008, pp. 822–824, doi: 10.1109/KAMW.2008.4810617.
[49] K. E. Petersen, "Silicon as a mechanical material," *Proc. IEEE*, vol. 70, no. 5, pp. 420–457, May 1982, doi: 10.1109/PROC.1982.12331.
[50] M. Bao, *Analysis and Design Principles of MEMS Devices*. Amsterdam, The Netherlands: Elsevier, 2005.
[51] S. Li *et al.*, "Bi-resonant structure with piezoelectric PVDF films for energy harvesting from random vibration sources at low frequency," *Sens. Actuators A, Phys.*, vol. 247, pp. 547–554, Aug. 2016, doi: 10.1016/j.sna.2016.06.033.

Anxin Luo received the B.Eng. degree in microelectronics and engineering from the Southern University of Science and Technology (SUSTech), Shenzhen, China, in 2017. He is currently pursuing the joint Ph.D. degree with the School of Microelectronics, SUSTech, and the Institute of Microelectronics, University of Macau (UM). His current research interests include energy harvester design and fabrication and power management circuit design for energy harvester.

Yulong Zhang received the B.S. degree in physics from Taiyuan Normal University, Taiyuan, China, in 2011, and the M.S. degree in physical electronics from the Xi'an University of Technology, Xi'an, China, in 2014. From 2015 to 2019, he was a Research Assistant with the Department of Electrical and Electronic Engineering, Southern University of Science and Technology, Shenzhen. Since 2019, he has been the Technician with the College of New Materials and New Energies, Shenzhen Technology University. His current research interest includes the micro/nano fabrication process.

Xinge Guo (Graduate Student Member, IEEE) received the B.Eng. degree in microelectronics engineering from the Southern University of Science and Technology, China, in 2019. He is currently pursuing the Ph.D. degree with the Department of Electrical and Computer Engineering, National University of Singapore, under NUS Research Scholarship. His research interests include energy harvesting and self-powered sensor technologies for IoT applications.

Yan Lu (Senior Member, IEEE) received the B.Eng. and M.Sc. degrees in microelectronics from the South China University of Technology, Guangzhou, China, in 2006 and 2009, respectively, and the Ph.D. degree in electronic and computer engineering from The Hong Kong University of Science and Technology (HKUST), Hong Kong, SAR, China, in 2013.

In 2014, he joined the State Key Laboratory of Analog and Mixed-Signal VLSI, University of Macau, Macau, where he is currently an Associate Professor. He has authored/coauthored more than 80 peer-reviewed technical articles and one book entitled *CMOS Integrated Circuit Design for Wireless Power Transfer* (Springer) and edited one book entitled *Selected Topics in Power, RF, and Mixed-Signal ICs* (River Publishers). His research interests include wireless power transfer circuits and systems, highly-integrated power management solutions, and low-power analog circuits.

Dr. Lu is serving as a TPC Member for International Solid-State Circuits Conference (ISSCC) and Custom Integrated Circuits Conference (CICC). He was a recipient/co-recipient of the 2018 Macao Science and Technology Award (second prize, with the first prize vacancy), the IEEE Solid-State Circuits Society Pre-doctoral Achievement Award for the period of 2013–2014, the IEEE CAS Society Outstanding Young Author Award in 2017, and the ISSCC 2017 Takuo Sugano Award for Outstanding Far-East Paper.

Chengkuo Lee (Senior Member, IEEE) received the Ph.D. degree in precision engineering from The University of Tokyo in 1996. He is currently the Director of the Center for Intelligent Sensors and MEMS, National University of Singapore, Singapore. In 2001, he cofounded Asia Pacific Microsystems, Inc., where he was the Vice President. From 2006 to 2009, he was a Senior Member of the Technical Staff with the Institute of Microelectronics, A*STAR, Singapore. He has contributed to more than 350 peer-reviewed international journal articles.

Fei Wang (Senior Member, IEEE) received the B.S. degree in mechanical engineering from the University of Science and Technology of China, Hefei, China, in 2003, and the Ph.D. degree in microelectronics from the Shanghai Institute of Microsystem and Information Technology, Chinese Academy of Science, Shanghai, China, in 2008.

He was a Post-Doctoral Researcher with the Department of Micro- and Nano-technology, Technical University of Denmark, where he has been an Assistant Professor since 2010. Since 2013, he has also been an Associate Professor with the School of Microelectronics, Southern University of Science and Technology, China. He has contributed to more than 180 peer-reviewed international journal articles, in addition to four book chapters. His current research interests include micro energy harvesting, microelectromechanical systems and NEMS sensors, and semiconductor testing.

Dr. Wang served as a TPC Member for the International Conference on Solid-State Sensors, Actuators and Microsystems (Transducers 2017, Transducers 2019, and ETPC for Transducers 2021), the 13th International Conference on Nano/Micro Engineered and Molecular Systems (NEMS 2018), and the International Conference on Manipulation, Manufacturing and Measurement on the Nanoscale (IEEE 3M-NANO) from 2014 to 2019.